nature communications

Article

https://doi.org/10.1038/s41467-026-75442-6

An integrated, scaled approach to resolve TSC2 variants of uncertain significance

Received: 16 January 2026

Accepted: 1 July 2026

Published online: 09 July 2026

Check for updates

Carina G. Biar[1,11], Ziyu R. Wang[2,11], Nathan D. Camp[3,11], Daniel L. Holmes[2], Melinda K. Wheelock[2], Sriram Pendyala[2], Abby V. McGee[2], Pankhuri Gupta[2], Abbye E. McEwen[2,4], Malvika Tejura[2], Marcy E. Richardson[5], Jamie D. Weyandt[5], Taylor Coleman[5], Alan F. Rubin[6,7], Nick Moore[6], Ross Stewart[8], Daniel Zeiberg[8], Allyssa J. Vandi[2], Samantha Dawson[3], Predrag Radivojac[8], Lea M. Starita[2,4], Gemma L. Carvill[1], Richard G. James[3,9,11] ✉, Douglas M. Fowler[2,4,10,11] ✉ & Jeffrey D. Calhoun[1,11] ✉

Obtaining a precise genetic tuberous sclerosis complex diagnosis is a challenge as many missense *TSC2* variants are variants of uncertain significance. Variants of uncertain significance in *TSC2* have been resolved by one-at-a-time functional assays, but these assays cannot scale to the 3634 *TSC2* missense variants of uncertain significance observed so far. To address this challenge, we use massively parallel sequencing to measure the steady-state abundance of almost 9000 *TSC2* missense variants and develop an mTOR pathway activity assay using genome editing and cell sorting to generate activity scores for 391 missense variants. We observe that 1256 of 8864 (14.17%) missense variants assayed have altered TSC2 abundance, and 69 of 391 (17.65%) missense variants assayed have altered mTOR pathway activity. Calibration and integration of these data into classification of variants identified in a clinical cohort putatively reclassifies 212 of 276 (76.8%) *TSC2* missense variants of uncertain significance. These datasets will lead to improved genetic diagnosis of tuberous sclerosis complex with potential positive impacts on the clinical management of patients and their families.

Tuberous sclerosis complex (TSC) is a genetic disorder affecting multiple organ systems including the brain, lung, kidneys, and skin. Hallmark manifestations include, but are not limited to, epilepsy and benign tumors. TSC is caused by pathogenic variants in two mTOR pathway genes, *TSC1* and *TSC2*[1,2]. *TSC1* and *TSC2* are also listed on the American College of Medical Genetics (ACMG) secondary finding list, as driver mutations in these genes are associated with increased risk for developing certain cancers such as early-onset renal cell carcinoma[3]. TSC2 interacts with TSC1 and the TSC1-TSC2 complex (TSCC) acts as a negative regulator of mechanistic target of rapamycin complex 1 (mTORC1) signaling[4]. The TSCC is a GTPase-activating protein with specific activity for Rheb, a GTPase which modulates

[1]Ken and Ruth Davee Department of Neurology, Northwestern Feinberg School of Medicine, Chicago, IL, USA. [2]Department of Genome Sciences, University of Washington, Seattle, WA, USA. [3]Center for Immunity and Immunotherapies, Seattle Children's Research Institute, Seattle, WA, USA. [4]Brotman Baty Institute for Precision Medicine, Seattle, WA, USA. [5]Ambry Genetics, Aliso Viejo, CA, USA. [6]Bioinformatics Division, The Walter and Eliza Hall Institute of Medical Research, Parkville, VIC, Australia. [7]Collaborative Centre for Genomic Cancer Medicine, University of Melbourne, Melbourne, VIC, Australia. [8]The Institute for Experiential AI, Northeastern University, Boston, MA, USA. [9]Department of Pediatrics and Pharmacology, University of Washington, Seattle, WA, USA. [10]Department of Bioengineering, University of Washington, Seattle, WA, USA. [11]These authors contributed equally: Carina G. Biar, Ziyu R. Wang, Nathan D. Camp, Richard G. James, Douglas M. Fowler, Jeffrey D. Calhoun. ✉e-mail: rickerj@u.washington.edu; dfowler@uw.edu; jeffrey.calhoun@northwestern.edu

https://doi.org/10.1038/s41467-026-75442-6

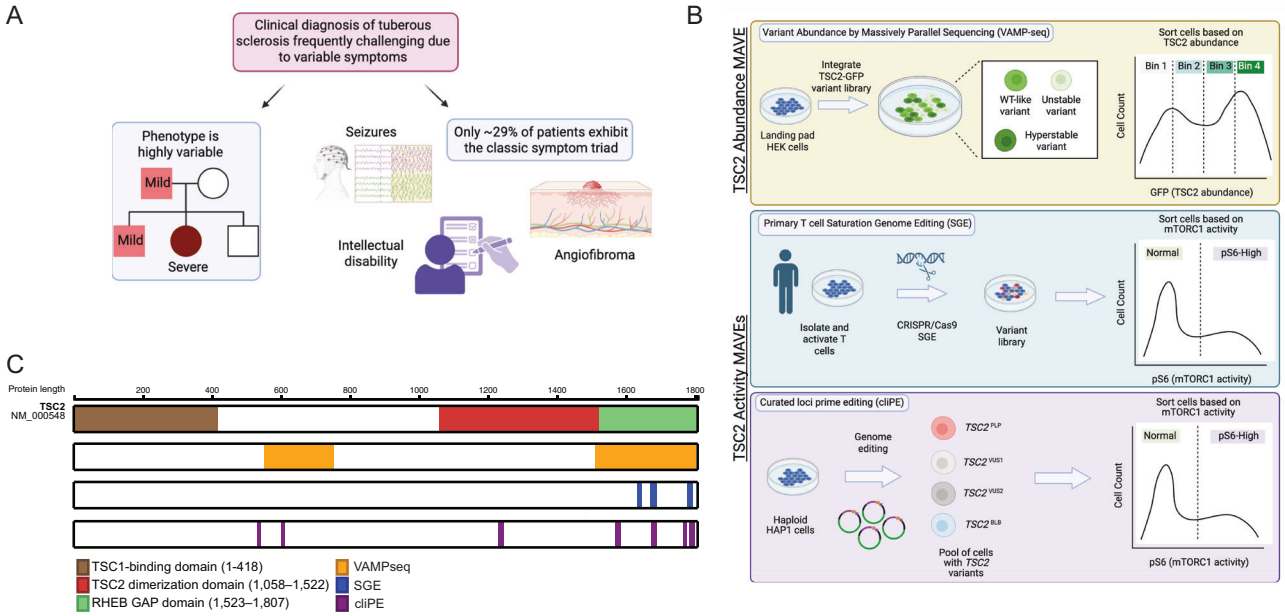

Fig. 1 | Prioritization of tuberous sclerosis complex related gene *TSC2* for generation of multiplexed assays of variant effect. A Major factors influencing prioritization of *TSC2* for MAVE development. Created in BioRender. Calhoun, J. (2026) https://BioRender.com/9epqzkz. **B** Introduction of three TSC2 MAVEs. Variant effect data for TSC2 abundance were generated using a VAMP-seq workflow. Two independent assays of TSC2 activity were performed in both primary donor T cells as well as HAP1s. Created in BioRender. Calhoun, J. (2026) https://BioRender.com/6iwt6aw. **C** Diagrams demonstrating known functional domains of TSC2 as well as the regions targeted by the TSC2 MAVEs reported herein.

mTORC1 activity[5]. The protein-protein interaction between TSC1 and TSC2 stabilizes TSC2 in the cell[6]. The TSC2 C-terminal Rheb GAP domain regulates catalytic activity of RHEB[5]. Protein structure studies describe the TSCC as having a scorpion-like or arch-shaped structure composed of a TSC1 dimer, a TSC2 dimer, and a single molecule of TBC1D7[7,8]. A particular key residue, N1643, is the asparagine thumb which mediates the Rheb GAP activity of TSC2[8,9].

Genetic diagnosis plays a major role in confirmation of a clinical diagnosis of TSC which can be challenging due to phenotype variability (Fig. 1A)[10,11]. Genetic diagnosis of TSC increases access to precision treatments such as rapamycin analogs which inhibit mTOR[12]. Of the 5011 missense variants of *TSC2* in ClinVar, 174 (3.47%) are pathogenic or likely pathogenic (PLP), 223 (4.45%) are benign or likely benign (BLB), but 4614 (92.08%) are either variants of uncertain significance (VUS) or have conflicting classifications. VUS arise when there is insufficient evidence to classify a variant as either pathogenic or benign or, more rarely, when there is conflicting evidence. Some *TSC2* VUS have been resolved by adding evidence from low-throughput functional studies in cell-based assays[13–19]. This important work describing how *TSC2* missense variants impact mTORC1 activity and TSC2 protein abundance in cell-based assays is the current gold standard and has been used for many years to inform variant classification. However, the rapid accumulation of VUS is incompatible with the throughput of these classical cell-based assays. Meanwhile, multiplexed assays of variant effect (MAVEs), which harness high-throughput DNA sequencing to functionally characterize thousands of variants simultaneously, offer a tangible solution[20].

We developed two complementary MAVE-based approaches to resolve *TSC2* VUS (Fig. 1B, C; Table 1). Some pathogenic TSC2 missense variants exhibit reduced protein abundance in heterologous systems, making abundance a promising molecular phenotype for identifying benign and pathogenic variants[13–16,19]. Additionally, TSC2 functions as a negative regulator of mTORC1 signaling, making phosphorylation of the mTORC1 effector S6 (pS6) a direct readout of TSC2 activity. To measure TSC2 protein abundance, we employed variant abundance by massively parallel sequencing (VAMP-seq), which measures steady-state protein abundance by fusing variants to GFP followed by fluorescence-activated cell sorting (FACS) and sequencing[21]. To assess TSC2 activity, we used endogenous genome editing combined with FACS for pS6, similar to our previous work on another mTOR pathway gene, *SZT2*[22]. The editing approach overcomes the inability of VAMP-seq to capture splicing variants. Given the variable phenotypic

Table 1 | Overview of three TSC2 MAVE datasets

	VAMP-seq	SGE	cliPE
Library type	cDNA	Genome editing (CRISPR/Cas9)	Genome editing (prime editing)
Coverage	Saturation	Saturation	Targeted
TSC2 variants (Total missense)	8,864	268	153
Selection	TSC2 abundance	TSC2 activity (mTORC1 activity via pS6 FACS)	TSC2 activity (mTORC1 activity via pS6 FACS)
Cell line/type	Landing pad HEK 293T	Primary donor T cells	HAP1
Codons targeted	554–757 1512–1805	1633–1646 1672–1689 1777–1793	534–543 602–611 1232–1246 1571–1584 1675–1686 1766–1777 1785–1797

VAMP-seq regions were selected with a primary focus on the Rheb GAP domain. In addition to its known functional role, the Rheb GAP region is enriched for known pathogenic missense variants. However, pathogenic missense variants are scattered across TSC2. As such, we included an additional N-terminal region spanning known recurrent pathogenic missense variants at residue R611. cliPE regions were selected primarily based on the density of missense VUS present in ClinVar[24]. The regions for SGE were primarily chosen based on recent protein structure studies detailing the TSC2 Rheb GAP domain[8,9]. Based on these studies, we chose a region surrounding key active site residue N1643. We also prioritized regions covered in VAMP-seq to maximize our ability to generate both abundance and activity data for as many residues as possible, and selected two other regions in the Rheb GAP domain for this purpose. We also prioritized overlapping at least one region with cliPE to investigate possible cell-type-specific variant effects.

presentation of TSC even among individuals with identical variants, we implemented these TSC2 activity assays in two cell types. In primary T cells isolated from healthy donors, we used a cloning-free saturation genome editing (SGE) approach[23]. In haploid HAP1 cells, we employed curated loci prime editing (cliPE), which uses prime editing to target specific regions enriched for VUS[24].

We measured the effect of 9812 missense, synonymous, and nonsense variants on abundance using VAMP-seq and 522 variants on pS6 levels using SGE and cliPE. We observed that 1256 missense variants reduced TSC2 abundance and 69 missense variants reduced TSC2 activity. Of these 69 variants, 34 altered both TSC2 abundance and mTORC1 activity. However, 31 variants reduced TSC2 activity but not abundance, and these variants clustered around the active site of the Rheb GAP domain. To reassess *TSC2* VUS, we developed a decision tree-based model to combine data from the assays. This model makes an initial assignment based on TSC2 abundance. Variants with an initial classification of functionally normal or indeterminate are replaced if SGE or cliPE data for that variant exists. OddsPath calibration is used to assign evidence strength, which varies from moderate evidence of benignity to strong evidence of pathogenicity depending on which assay is used for the final classification within the decision tree. We tested our decision tree method using 340 variants from a clinical cohort derived from a large commercial genetic diagnostic laboratory with an ACMG/AMP variant classification framework. We putatively classified 199 (72.1%) variants as likely benign, 13 (4.7%) as pathogenic/likely pathogenic, and 64 (23.1%) remained VUS. PS3/BS3 functional evidence codes derived from TSC2 MAVE data contributed to 91% (193/212) of classifications. Herein, we report the results of these three TSC2 MAVE datasets and discuss how these data will facilitate the resolution of missense *TSC2* VUS.

Results

Development of multiplexed assays of variant effect for TSC2

Based on previous reports demonstrating loss of variant abundance as a common pathogenic mechanism for *TSC2* missense variants, we were interested in developing a high-throughput assay of TSC2 abundance[13–19]. VAMP-seq, a well-validated and high-throughput assay of variant effects on protein abundance, utilizes a library of barcoded, fluorescently-tagged variants integrated at single copy in the host genome of cells using a defined landing pad and Bxb1-mediated integration (Fig. 1B)[21]. Pilot VAMP-seq experiments showed WT TSC2-GFP expressing cells were separable from cells expressing a premature termination codon (PTC) variant (Supplementary Figs. 1, 2). Cells expressing a pilot library of the WT reference TSC2 allele and 47 unique variants ($n = 20$ PTC variants; $n = 27$ missense variants) were distributed broadly with a peak corresponding to cells with low TSC2-GFP abundance (Supplementary Fig. 3). We sorted cells into bins based on GFP fluorescence and performed amplicon sequencing to confirm that WT expressing cells were enriched in high GFP bins while PTC variants were enriched in low GFP bins (Supplementary Fig. 4). Based on these results, we proceeded to perform VAMP-seq at saturation scale (Supplementary Figs. 5, 6). We selected two regions of TSC2 to focus on (Table 1): (1) an N-terminal region containing residue 611 with four recurrent pathogenic missense variants and (2) the full Rheb GAP domain, a domain critical for the TSCC's negative regulation of mTORC1 activity. We normalized the TSC2 abundance data such that increasing scores approaching 1 indicate normal abundance whereas low scores near 0 indicate low abundance[21]. Synonymous TSC2 variants ($n = 364$) were distributed with a relatively narrow range of scores (mean = 0.992; standard deviation = 0.103) (Fig. 2A). In contrast, the scores for missense variants ($n = 8864$) were bi-modally distributed (mean = 0.755; standard deviation = 0.348), with one subpopulation overlapping synonymous variants. Some missense variants had intermediate abundance scores (<0.75 and >0.25), suggesting that they may be hypomorphic in terms of protein abundance. We observed that 1256 of 8864 (14.17%) missense variants had low abundance (<0.25) in the VAMP-seq assay. For example, the known recurrent pathogenic missense variants at position 611 (R611W, R611Q, and R611G) all exhibit loss of abundance. Of the remaining variants, 5530 (62.39%) missense variants had normal abundance; the remaining 1854 (20.92%) missense variants were considered indeterminate. We investigated whether any missense variants might exhibit increased abundance and found that 224 (2.53%) missense variants may have increased protein abundance (TSC2 abundance >= 1.2, exceeding two standard deviations above the mean for synonymous variants). However, it is unclear if these variants impact TSC2 activity. Only one variant (p.Gly1642 Asp) among these is known to be pathogenic and had low activity in the SGE assay. To better visualize the nuanced relationships between individual substitutions and abundance, we plotted the abundance of each possible amino acid by row and each numbered TSC2 residue by column as a heatmap (Fig. 2B). The example here was selected to highlight R611 with multiple recurrent PLP variants (see Supplementary Figs. 5, 6 for comprehensive heatmaps of all substitutions assayed).

We designed TSC2 activity MAVEs around genome editing of the endogenous *TSC2* locus by either cloning-free SGE or prime editing followed by sorting cells by the abundance of pS6, a biomarker of mTORC1 activity (Fig. 1B)[23,24]. Based on prior work with mTOR pathway member *SZT2*, we anticipated edited cells with variants causing loss of TSC2 activity would be enriched in cells with high levels of pS6[22]. As a proof-of-concept for a TSC2 activity MAVE, we first performed pilot experiments with a single guide RNA targeting *TSC2* exon 17. We demonstrated that cells with nonhomologous end joining induced indels causing frameshifts and therefore loss of TSC2 activity had higher levels of pS6 relative to untransfected cells (Supplementary Figs. 7, 8). Based on this, we next generated libraries of variants using two methods in both primary T cells and HAP1 cells to capture potential cell-type specific variant effects. Regions targeted for cliPE were selected using 10 codon stretches with maximal density of VUS present in ClinVar[24]. Recent structural studies guided the selection of regions targeted for SGE to focus on active site residues within the Rheb GAP domain[8,9]. We generated TSC2 activity scores for 522 variants, including 391 missense variants, 64 synonymous variants, and 67 PTC variants (Supplementary Figs. 9, 10). In these activity MAVEs, the score based on mTORC1 activity is inversely proportional to TSC2 activity, as TSC2 is a negative regulator of MTOR. Thus, larger scores indicate low TSC2 activity (high pS6 level; mTORC1 active; TSC2 inactive), and vice versa.

The activity scores of synonymous and PTC variants comprised distinct populations with non-overlapping distributions, showing these assays distinguished functionally normal from functionally abnormal variants (Fig. 2A). The activity score distributions for all missense variants were bimodal with one mode overlapping the synonymous variant distribution and the other overlapping the PTC variant distribution, revealing that some missense variants retain activity while others have abnormal activity. We observed that 52 of 268 (19.4%) missense variants exhibited abnormal activity in the SGE assay while 22 of 153 (14.38%) missense variants had abnormal activity in the cliPE assay. Known recurrent pathogenic missense variants at position 611 (R611W, R611Q, and R611G) all exhibit loss of activity in the cliPE assay. Similarly as above for abundance, we plotted the activity of each possible amino acid by row and each numbered TSC2 residue by column as a heatmap (Fig. 2B). The SGE example shown here was selected to highlight one of the Rheb GAP regions assayed (see Supplementary Fig. 9 for comprehensive heatmaps of all substitutions assayed). The cliPE example shown here was selected to highlight R611 with multiple recurrent PLP variants and show overlapping assayed variants with VAMP-seq (see Supplementary Fig. 10 for comprehensive heatmaps of all substitutions assayed).

https://doi.org/10.1038/s41467-026-75442-6

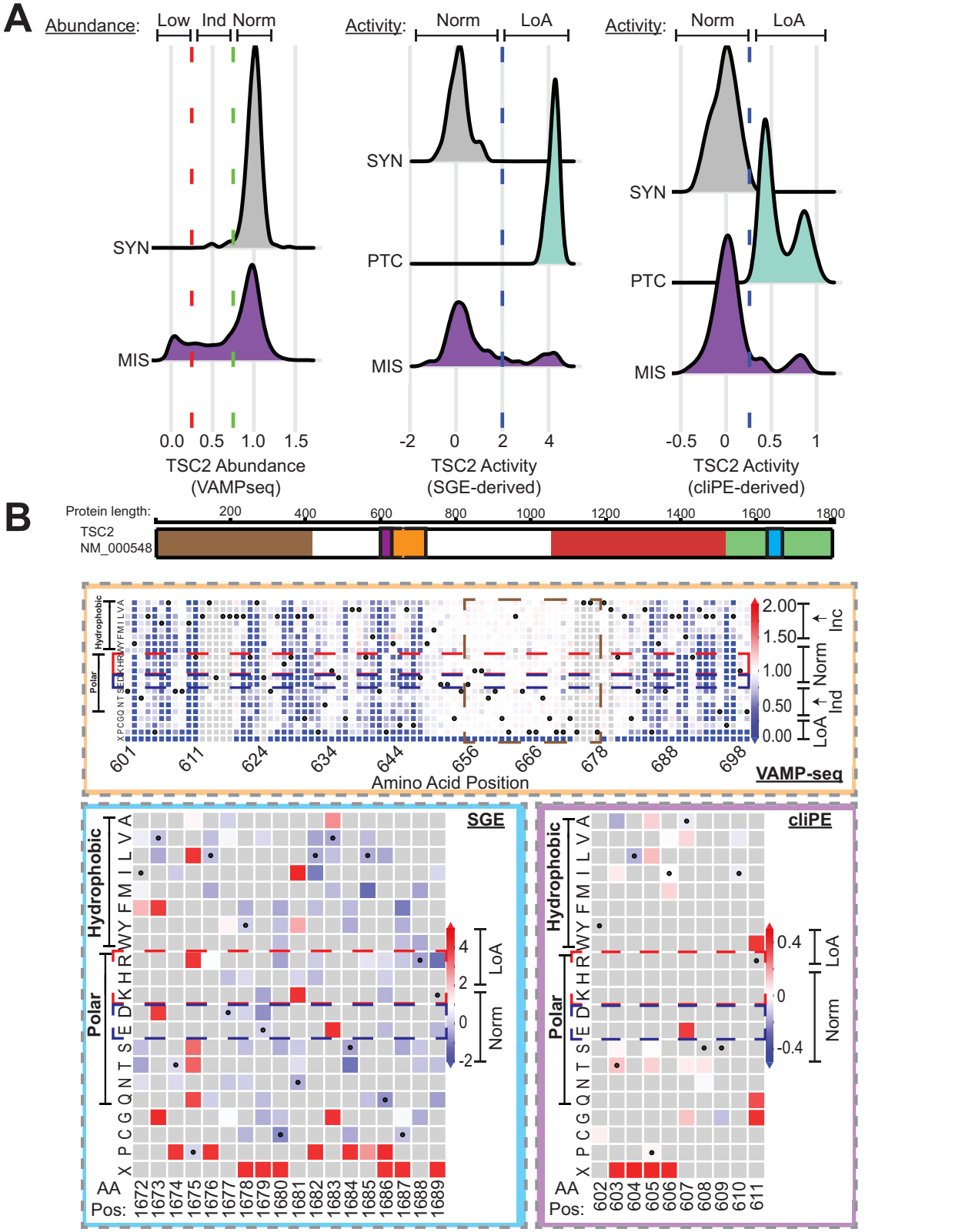

TSC2 variant abundance and activity are strongly correlated

We next analyzed the relationship between TSC2 variant abundance (VAMP-seq) and activity as measured in primary T cells and HAP1 cells (Fig. 3). Abundance was strongly correlated with activity in primary T cells (Pearson correlation = −0.57) and in HAP1 cells (Pearson correlation = −0.69, Fig. 3A, C). The SGE and cliPE datasets correlate very strongly with a coefficient of 0.92, suggesting few if any cell-type-specific variant effects (Supplementary Fig. 11). Thus, the majority of variants have concordant effects on abundance and activity as well as on activity between cell types. We observed 31 variants which exhibited normal abundance yet reduced activity, and we hypothesized that these variants directly impacted TSC2 catalytic activity. Indeed, these were located near the active site of the Rheb GAP domain (Fig. 3B, D)[9]. Only residues within an alpha helix, the

https://doi.org/10.1038/s41467-026-75442-6

Fig. 2 | TSC2 variant abundance and activity mapping. A Distributions of variant effect scores by variant class. (Left) The threshold for low abundance is denoted by a vertical red dotted line while the threshold for normal abundance is designated by the vertical green dotted line. The regions of scores corresponding to low, indeterminate, or normal abundance are also annotated above the plot. (Middle and right) The threshold separating variants with normal or low TSC2 activity is denoted by a vertical blue line and the corresponding regions are further annotated above each plot. SYN synonymous, PTC premature termination codon, MIS missense, Norm normal, Ind indeterminate, LoA loss-of-activity. **B** Example heatmaps showing individual variant effect scores by amino acid position for each of the three assays. Heatmaps comprehensive of all variants assayed are presented as Supplementary Figs.. Colored highlighting behind heatmaps designate which assay is shown based on color in Fig. 1C (VAMP-seq in orange; cliPE in purple; SGE in light blue). Amino acid residues are grouped by biochemical properties. Positively charged residues are annotated with a red box with dotted lines and negatively charged residues are annotated with a blue box with dotted lines. A disordered region is annotated with a brown box with dotted lines; substitutions within and adjacent to this disordered region have little to no effect on TSC2 abundance. The reference amino acid for each position is annotated with a small black circle. The color map of each heatmap is annotated with the thresholds for each assay. Gray boxes denote a variant that was not assayed. Norm Normal TSC2 abundance or activity, LoA low abundance (VAMP-seq) or loss-of-activity (cliPE/SGE), Ind indeterminate abundance, Inc increased abundance.

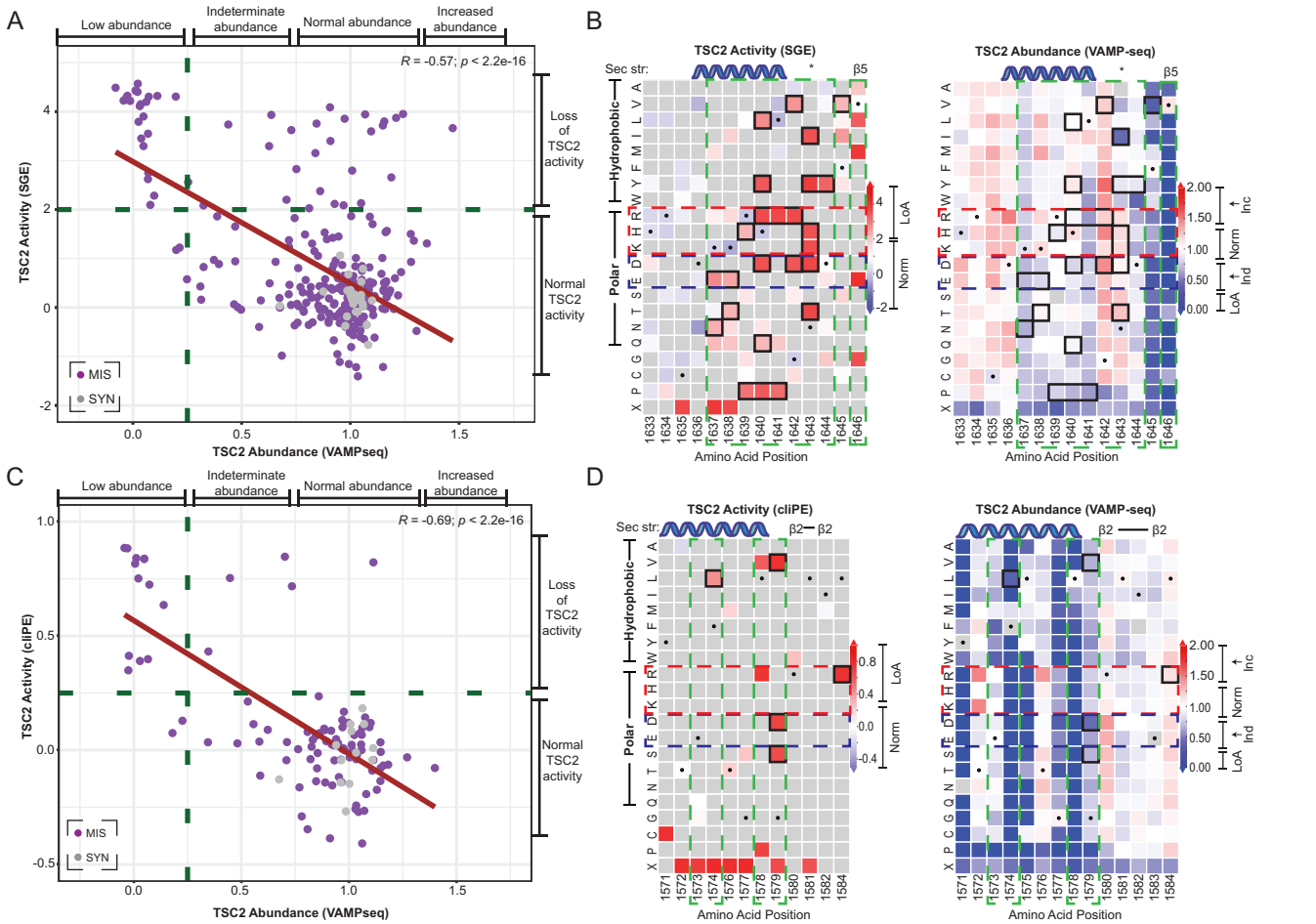

Fig. 3 | TSC2 abundance and activity are strongly correlated. A Scatterplot and pairwise correlation (Pearson) of the VAMP-seq TSC2 abundance dataset with the SGE TSC2 activity dataset. Solid red line is the line of best fit. Dotted lines and text annotation indicate the assay thresholds separating variants with normal abundance or activity from those with altered abundance or activity. Purple dots indicate missense (MIS) variants while gray dots indicate synonymous (SYN) variants. Synonymous variants fall within the quadrant of the plot with normal abundance and normal activity. **B** Heatmaps showing all variant effect scores spanning amino acid residues 1633–1646 of the Rheb GAP domain for VAMP-seq and SGE datasets. Variants meeting criteria for loss of TSC2 activity without concomitant loss of TSC2 abundance are shown highlighted with black squares. Heatmaps are annotated as described in Fig. 2B with the following exceptions: (1) secondary structure is annotated above each heatmap to show amino acids which form either an alpha helix, a linker region, or a beta sheet, (2) asterisk (*) designates the asparagine residue (p.N1643) which is a critical active site for Rheb GAP domain function, (3) regions of high evolutionary conservation are annotated with a green box with dotted lines; most substitutions within and adjacent to this region have little to no effect on TSC2 abundance. **C** Scatterplot and pairwise correlation (Pearson) of the VAMP-seq TSC2 abundance dataset with the cliPE TSC2 activity dataset. Annotations as described in panel (**A**). Synonymous variants fall within the quadrant of the plot with normal abundance and normal activity. **D** Heatmaps showing all variant effect scores spanning amino acid residues 1571–1584 of the Rheb GAP domain for VAMP-seq and cliPE datasets. Annotations of the heatmap plots are as described in panel (**B**).

beginning of the adjacent beta sheet, or the linker region between these two secondary structure elements resulted in reduced activity variants that retained normal abundance. Of these inactive yet abundant variants, all but one mapped to highly evolutionarily conserved residues.

We next investigated the relationship between our multiplexed TSC2 measurements and measures of evolutionary conservation. VAMP-seq abundance measurements weakly correlated (Pearson correlation coefficients between −0.18 and −0.29) with evolutionary conservation metrics (Fig. 4A). Activity scores were weakly to

https://doi.org/10.1038/s41467-026-75442-6

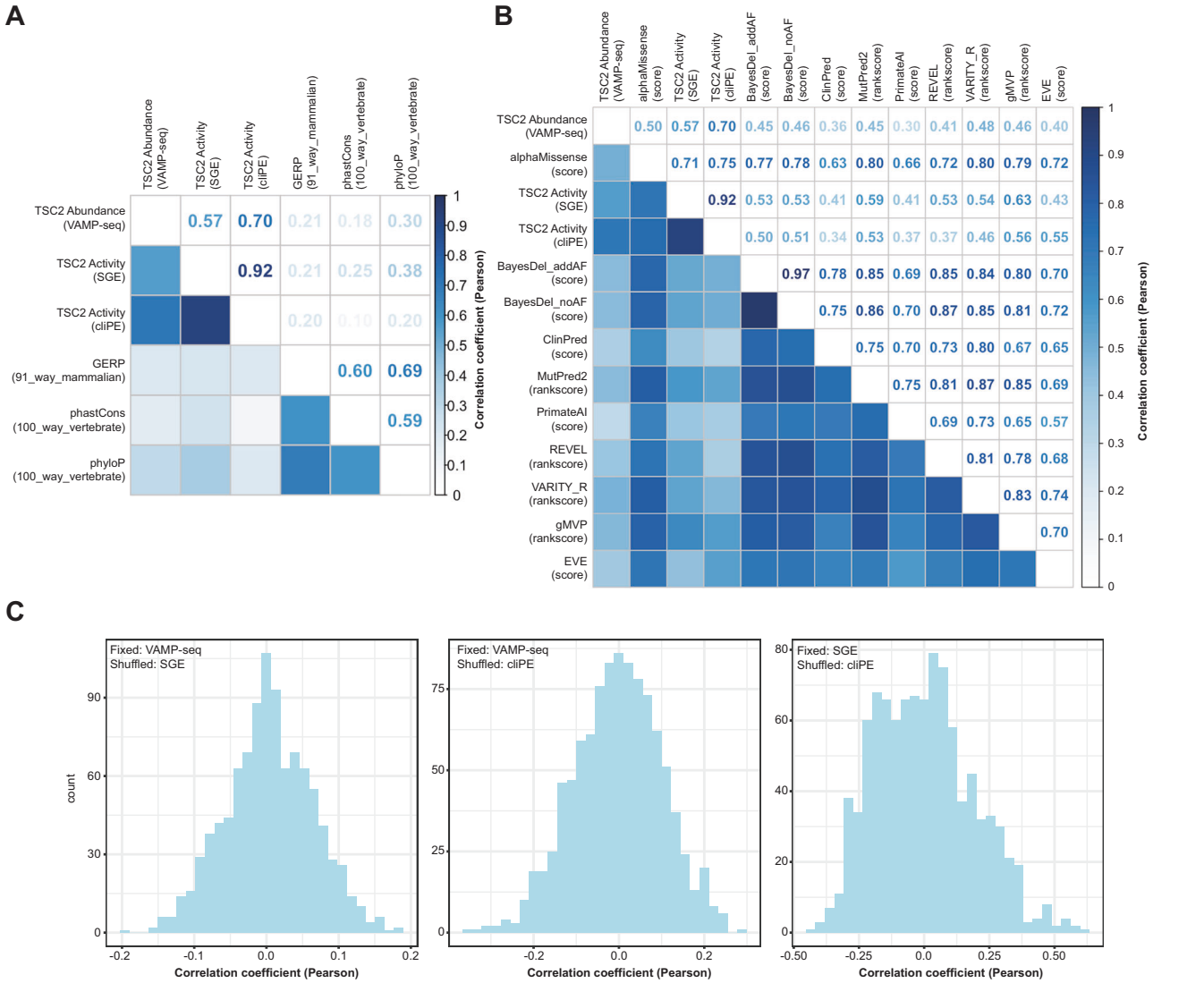

Fig. 4 | Correlation of TSC2 MAVEs with evolutionary conservation metrics and variant effect predictors. A Correlation plot of TSC2 MAVE datasets and evolutionary conservation metrics. **B** Correlation plot of TSC2 MAVE datasets and variant effect predictors. In both panel (**A**) and panel (**B**), the inverse of the TSC2 abundance VAMP-seq score was used to calculate correlation coefficients in the first column. **C** Randomization test of correlations. Pairwise for each MAVE, we fixed one scoreset and randomly shuffled the other scoreset and calculated the correlation coefficient (Pearson). This was repeated 1000 times to generate a null distribution of correlation coefficients. In each case, the distributions were centered around 0. The observed correlation coefficients for unshuffled data do not overlap with the null distributions.

moderately correlated (Pearson correlation coefficients between 0.1 and 0.38) with measures of evolutionary conservation (Fig. 4A). We used a pairwise randomization test where one scoreset was fixed and the other was randomly shuffled. This randomization was repeated 1000 times and at each iteration the Pearson correlation coefficient was computed to generate a null distribution of correlation coefficients. An example of this is shown for each TSC2 MAVE in Fig. 4C (please see Supplementary Figs. 12–15 for all null distributions). The 0.1 correlation coefficient for cliPE and phastCons may be random as this falls within the null distribution (Supplementary Fig. 12). The remaining correlation coefficients either fall on the extreme end of the null distribution or fall well outside the null distribution, which demonstrates that the observed relationships are not due to chance.

We next asked whether our multiplexed TSC2 measurements correlated with variant effect predictor (VEP) scores. Previous analyses find that MAVE data often correlates with VEP scores, though the strength of this correlation varies by MAVE and by VEP[25,26]. We observed that TSC abundance moderately correlated with VEP scores (Pearson correlation coefficients ranging between −0.3 and −0.497); AlphaMissense showed the strongest negative correlation among VEPs (Fig. 4B)[27]. In general, activity scores were positively correlated with VEP scores, with AlphaMissense having the strongest correlation (Pearson correlation coefficients between 0.34 and 0.75; AlphaMissense/SGE = 0.71, AlphaMissense/cliPE = 0.75). We found that all of the correlation coefficients computed fall well outside their respective null distribution; this provides statistical evidence supporting the relationships between TSC2 MAVE scores and VEP predictions (Supplementary Figs. 13–15). Overall, AlphaMissense correlates most strongly with our abundance, SGE-derived activity, and cliPE-derived activity datasets, suggesting it may be the optimal VEP to calibrate and use to assign in silico pathogenicity evidence in an ACMG/AMP variant classification framework.

Approximately one-third of residues assayed for abundance were fully or partially intolerant to amino acid substitution

The VAMP-seq heatmaps suggested variability in tolerance to substitution across the regions assayed (Fig. 2B). We investigated this

https://doi.org/10.1038/s41467-026-75442-6

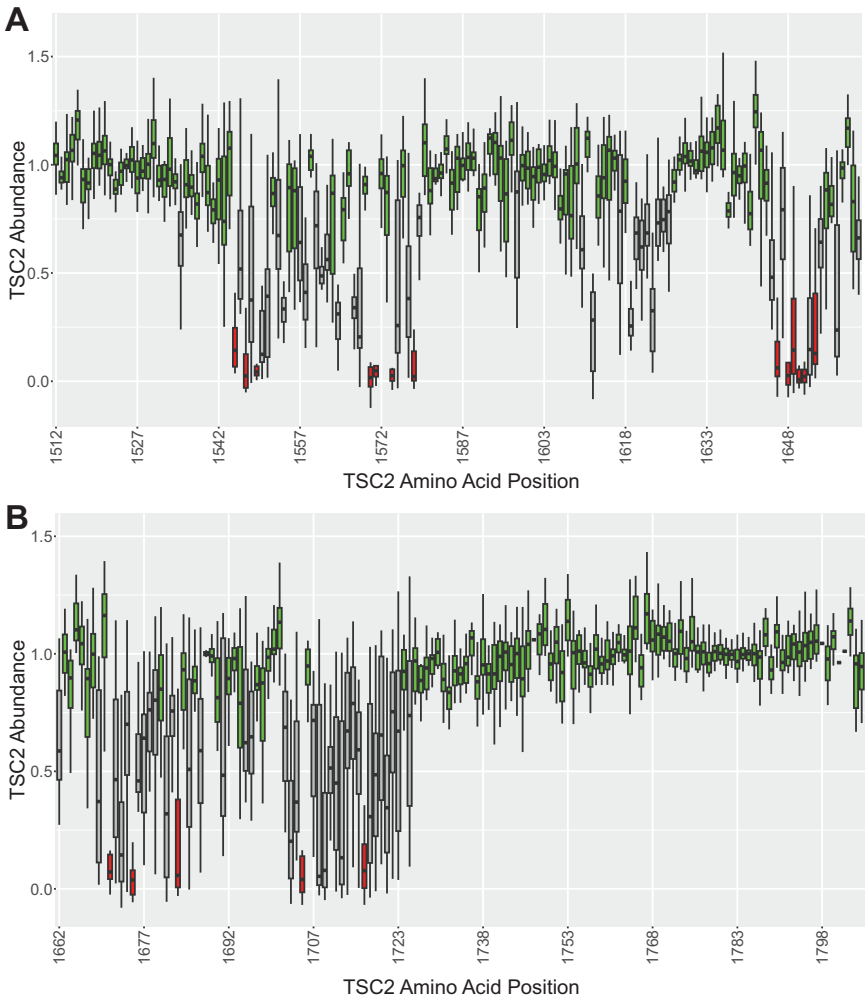

Fig. 5 | TSC2 Rheb GAP domain tolerance to substitution through a lens of variant effects on abundance. The abundance of all substitutions at each position is plotted as a boxplot with the center line as the mean. **A** Spans amino acids 1572–1722. **B** Spans amino acids 1723–1805. The lower and upper hinges correspond to the first and third quartiles, respectively. The upper and lower whiskers extend from the hinge to the largest or smallest value no further than 1.5 multiplied the inter-quartile range. Outlier values are not displayed. (Boxes are filled green if mean abundance is >0.75, or above the threshold for normal abundance. Boxes are filled gray if mean abundance is between 0.25 and 0.75, or within the indeterminate range. Boxes are filled red if mean abundance is less than 0.25, or below the thresholds for low abundance.

observation further and found that TSC2 residues could be broadly categorized in three groups: (1) tolerant to amino acid substitution (<20% of substitutions assayed resulting in loss of abundance), (2) partially tolerant to substitution (between 20 and 60% of substitutions result in low protein abundance), and (3) highly intolerant to substitution (>60% of substitutions result in low protein abundance). In total, 377 TSC2 residues were tolerant to amino acid substitution (Fig. 5; Supplementary Fig. 16). We identified 48 residues which were highly intolerant to amino acid substitution. The remaining residues ($n = 61$) partially tolerate substitution. To better understand these variants with reduced abundance, we analyzed them in the context of the AlphaFold2 predicted structure for TSC2. Many tolerant residues mapped to predicted disordered regions, such as between residue 650 and 680 (Fig. 2B). Similarly, many tolerant residues mapped to the C-terminal region spanning residues 1724–1805, which is mostly disordered. However, some predicted structured regions, such as the alpha helix spanning residues 704–716, contained multiple tolerant residues. Highly intolerant and partially tolerant residues mapped to structured regions including alpha helices (such as residues 582–598) and beta sheets (such as residues 1646–1651). Examples of residues highly intolerant and partially intolerant are 611 and 610, respectively. Residue 611 is a well-known residue in the TSC genetics field with 4 known ClinVar PLP variants (R611W, R611P, R611Q, and R611G).

TSC2 variant effect data improve genetic diagnosis of TSC by resolving missense VUS

We analyzed the abundance and activity scores of *TSC2* missense BLB ($n = 54$) and PLP ($n = 80$) control variants found in ClinVar (Fig. 6). For both abundance and activity scores, BLB and PLP controls minimally overlapped, with the exception of a proportion (31/80; 38.75%) of PLP variants with normal abundance. The separation of PLP and BLB variants by abundance and activity scores suggested that the data would have utility for variant classification and VUS resolution. We further confirmed this in the VAMP-seq abundance data using a unique set of missense variants curated from LOVD, a well-curated database of *TSC2* variants, and general population databases which would be expected to be enriched for PLP and BLB variants, respectively (Supplementary Fig. 17).

The original Richards et al. ACMG/AMP variant classification framework which has been widely adopted allows for the use of a "well-established functional assay" as evidence towards pathogenicity (PS3) or benignity (BS3)[28]. However, precise guidance on what criteria qualifies an assay as "well-established" and what strength of evidence to

https://doi.org/10.1038/s41467-026-75442-6

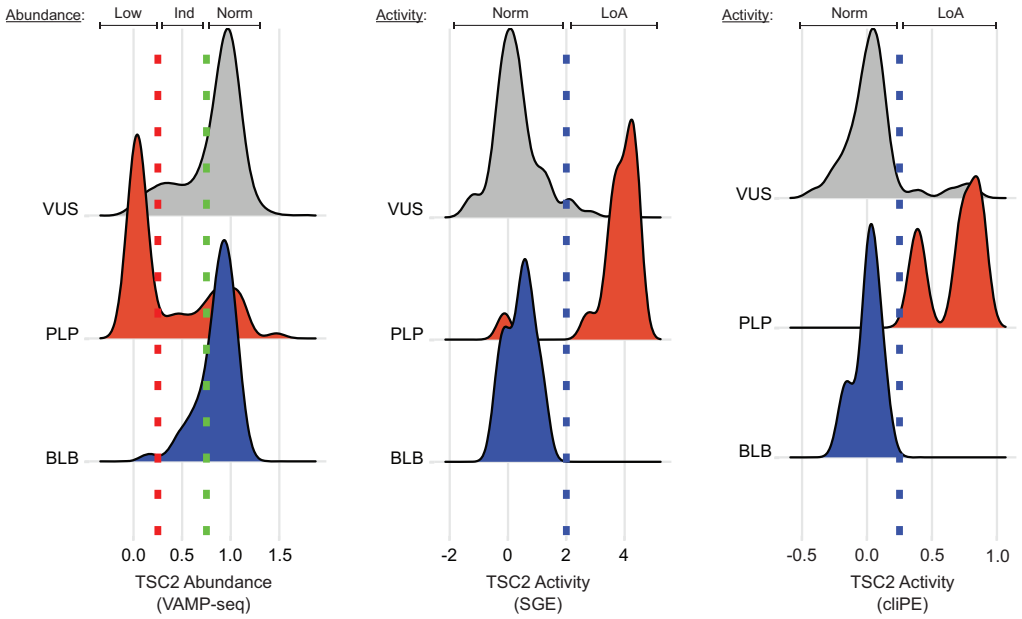

Fig. 6 | ClinVar variants of known pathogenicity or benignity have distinct distributions across TSC2 MAVE datasets. Distributions of variant effect scores by ClinVar annotation. SYN synonymous, PTC premature termination codon, MIS missense, Norm normal, Ind indeterminate, LoA loss-of-activity, VUS variant of uncertain significance, PLP pathogenic or likely pathogenic, BLB benign or likely benign. (Left) The threshold for low abundance is denoted by a vertical red dotted line while the threshold for normal abundance is designated by the vertical green dotted line. The region of scores corresponding to low, indeterminate, or normal abundance are also annotated above the plot. (Middle and right) The threshold separating variants with normal or low TSC2 activity is denoted by a vertical blue line and the corresponding regions are further annotated above each plot.

Table 2 | Odds of pathogenicity (OddsPath) calculations for individual MAVE datasets

	ClinVar BLB	ClinVar PLP	OddsPath_PS3	OddsPath_BS3
VAMP-seq	54[a]	80	33.1 ('strong')	0.343 ('supporting')
SGE	6	16	5.6 ('moderate')	0.094 ('moderate')
cliPE	9	10	4.5 ('moderate')	0.113 ('moderate')

OddsPath ranges mapping to evidence strength are based on a Bayesian implementation of the ACMG/AMP variant classification framework[30,59]. OddsPath_PS3 values > 18.7 = strong evidence (VAMP-seq) in support of pathogenicity. OddsPath_PS3 between 4.3 and 18.7 = moderate evidence (cliPE and SGE) in support of pathogenicity. Similarly, OddsPath_BS3 values between 0.23 and 0.48 = supporting evidence (VAMP-seq) in support of benignity. OddsPath_BS3 values between 0.053 and 0.23 = moderate evidence (cliPE and SGE) in support of benignity.
[a]One ClinVar BLB variant, p.S641I, was excluded from these calculations; please see Discussion for rationale.

apply led to discrepancies in how PS3 and BS3 were applied by different clinical laboratories[29]. One widely used, and ClinGen-approved, framework to address this is the Odds of Pathogenicity (OddsPath) framework[30]. We evaluated the utility of functional data for preliminary reclassification of *TSC2* VUS using the OddsPath framework. In the OddsPath framework, an OddsPath calculation (Eq. (3)) is performed which assesses how well an assay performs at distinguishing known PLP and BLB missense variants from a truth set, a well-curated database of variant classifications. We calculated the strength of evidence generated by each dataset using the OddsPath approach (Table 2)[30]. Under this framework, reduced abundance variants receive strong evidence of pathogenicity (OddsPath 33.1; PS3_strong) and normal abundance variants receive supporting evidence of benignity (OddsPath 0.343, BS3_supporting). The VAMP-seq assay is not limited by truth set variants ($n = 134$) and no ClinVar BLB variants are classified as low abundance; taken together, these explain why the VAMP-seq assay meets the criteria for strong evidence of pathogenicity. Importantly, some ClinVar PLP variants retain normal abundance, which limits the VAMP-seq assay in terms of providing evidence exluding pathogenicity. Reduced activity variants in either the primary T cell or HAP1 activity assays received moderate evidence of pathogenicity (OddsPath 4.5,5.6; PS3_moderate) and normal activity variants in either assay received moderate evidence of benignity (OddsPath 0.113, 0.094; BS3_moderate). The primary limiting factor here is number of truth set variants evaluated (9 BLB and 10 PLP for cliPE; 6 BLB and 16 PLP for SGE). In the future, if these activity assays are expanded to include additional truth set variants, we predict they may meet criteria to be used at strong evidence strength for both pathogenicity and benignity.

To combine evidence from the abundance and activity assays, we developed a decision tree to guide how the data we present can be used in the ACMG/AMP framework (Fig. 7A). Variants are first assigned an initial PS3/BS3 evidence code based on the score for that variant in the abundance assay. Then, this PS3/BS3 evidence code is adjusted, if appropriate, based on the score of the variants in one of the activity assays. We chose this approach because more variants were scored in the abundance assay and this assay yields a higher maximum evidence strength for pathogenicity. Using calibrated functional data together with Ambry's evidence and computational predictions, 212 of 276 (76.8%) *TSC2* missense VUS with available functional data were putatively reclassified under ACMG/AMP (v3.0) criteria (Supplementary Data 1). Of these, 199 (72.1%) qualified as likely benign, 13 (4.7%) as pathogenic/likely pathogenic, and 64 (23.1%) remained VUS. Computational evidence contributed to 90.5% (192/212) reclassifications, and

https://doi.org/10.1038/s41467-026-75442-6

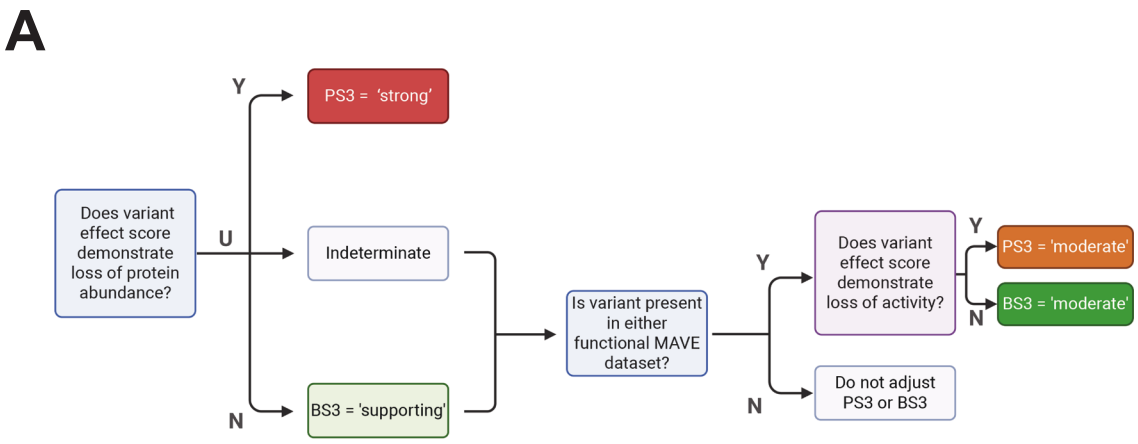

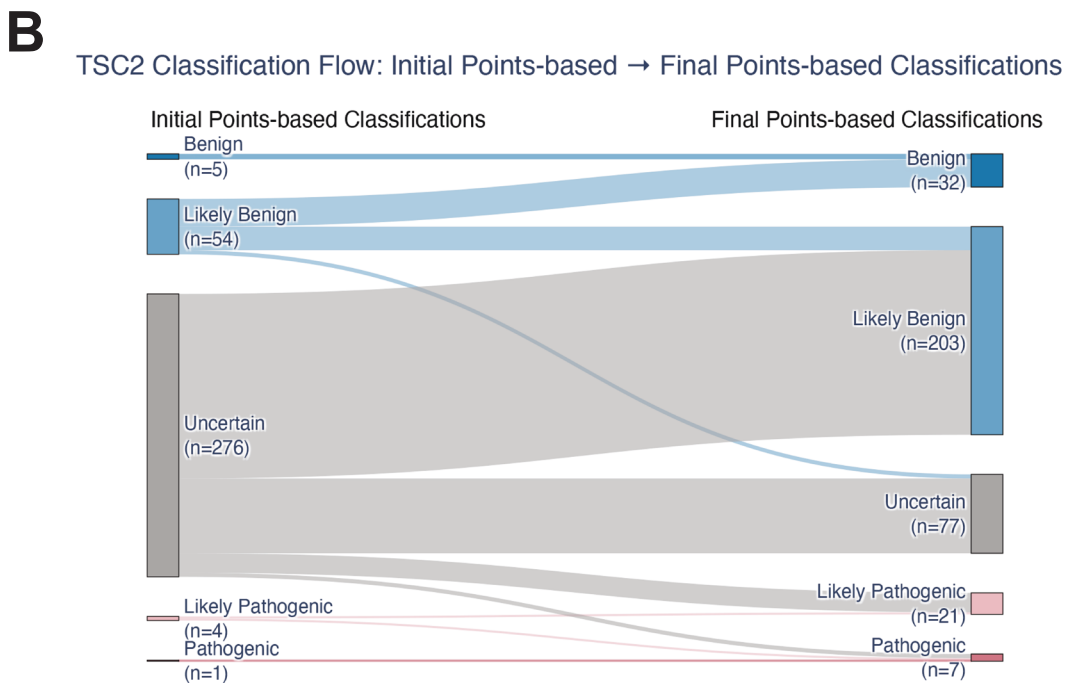

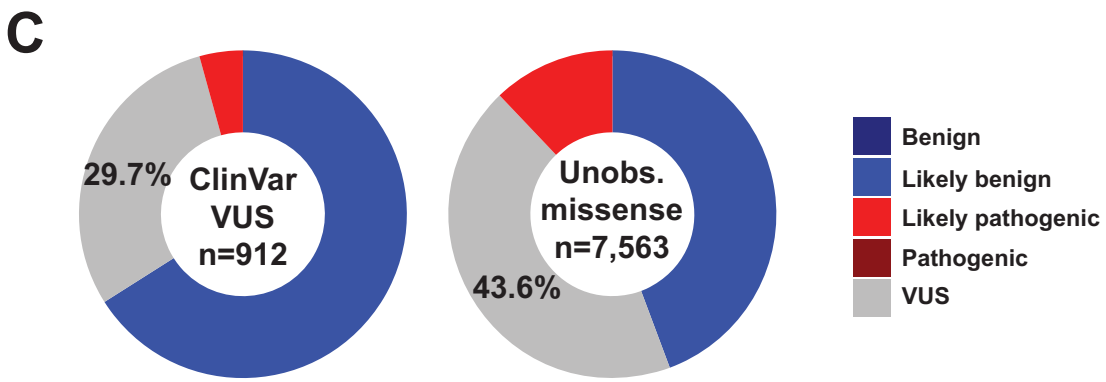

Fig. 7 | Employing TSC2 MAVE data for resolution of missense VUS in a standard framework. A Proposed decision tree for utilization of MAVE datasets during standard variant classification. Created in BioRender. Calhoun, J. (2026) https://BioRender.com/xp2cvv3. **B** Points-based implementation of ACMG/AMP (v3.0) variant classification for Ambry cohort. On the left are initial points-based classifications; on the right are final, putative points-based classifications using calibrated in silico VEP evidence and PS3/BS3 evidence derived from the decision tree in panel (**A**). This framework enabled putative reclassifications of VUS to either likely pathogenic or likely benign, as well as up- and downgrading some likely benign and likely pathogenic variants. Putative variant reclassification also summarized in Supplementary Table 2. **C** Putative variant classification using in silico VEP evidence and PS3/BS3 evidence codes derived from the decision tree in panel (**A**). BS3/PS3 evidence codes enable reclassification of missense variants to either likely pathogenic or likely benign.

functional data contributed to 91% (193/212). Variants remaining VUS had indeterminate functional results ($n = 31$), conflicting functional and computational evidence ($n = 23$), or insufficient evidence for reclassification ($n = 10$). The variant classification using this approach is shown in Fig. 7B.

Many variants in our MAVE datasets were not in our clinical dataset. Experimental and predictive data were used to determine whether MAVE data could move these variants from VUS to other categories (Supplementary Data 2 and Fig. 7C). Of 912 missense ClinVar VUS with variant effect data, we putatively classified 602 (66%) variants as likely benign, 271 (29.7%) variants as uncertain, and 39 (4.28%) variants as likely pathogenic. Predictive data were available for 865 (94.85%) of ClinVar missense VUS. We similarly investigated unobserved variants, or variants which have yet to be observed in an individual in gnomAD or ClinVar. Of 7563 unobserved missense variants, we assigned putative classifications of 3351 (44.31%) variants as likely benign, 2752 (36.39%) variants as uncertain, and 914 (12.09%) variants as likely pathogenic (Fig. 7C). Predictive data were available for 7516 (99.38%) unobserved missense variants.

Discussion

We developed three multiplexed assays to resolve *TSC2* VUS. We used VAMP-seq to measure the abundance of 8864 unique missense variants in an N-terminal portion of TSC2 and the full Rheb GAP domain (Fig. 8A). We used SGE and cliPE to measure S6 phosphorylation, a proxy for the activity of TSC2, on 522 variants in primary T cells and HAP1 cells, respectively (Fig. 8A). Our data revealed that some variants in the Rheb GAP domain cause loss of TSC2 activity with no change in protein abundance. This suggests that TSC2 activity and abundance data are complementary, which argues that generating variant effect data for both abundance and activity is optimal for *TSC2*. In a clinical cohort, we putatively reclassified more than 75% of VUS and variant effect data contributed to over 90% of the reclassifications, demonstrating the clinical utility of our MAVE datasets (Fig. 8B).

Our data can empower the precise genetic diagnosis of TSC by reducing VUS burden and by providing evidence to avoid future VUS. Reducing VUS in *TSC2* is clinically meaningful because PLP variant diagnosis can be used to prescribe mTOR inhibitor therapy, a first-line therapy for TSC[31]. In addition, resolving VUS to PLP can increase involvement in clinical trials for new precision therapies and empower family planning. Resolving VUS to BLB can eliminate worry, prevent unneeded treatment, or suggest the need for further genetic testing and clinical workup. It is worth emphasizing that, from a clinical genetics standpoint, the greatest strength of the TSC2 abundance variant effect dataset is detecting pathogenic variants (specificity = 98.18%). While the assay generates evidence towards benignity at supporting evidence strength (sensitivity = 61.25%), appropriate care must be taken when using this benign evidence for variant classification.

In the course of our work, we identified some possible errors within ClinVar. First, p.S641I, labeled as a low abundance variant by VAMP-seq, was classified as a benign variant in ClinVar. p.S641I has been previously published as a pathogenic missense variant and further listed as either likely pathogenic or pathogenic in multiple unique entries within the *TSC2* LOVD database[32,33]. Second, p.S540P, a variant with reduced TSC2 activity as measured in our cliPE assay, is listed as a benign variant in ClinVar. Lastly, p.Q1686K is listed as a likely pathogenic variant within ClinVar. We infer that the known pathogenic variant p.Q1686P likely contributed to this classification of p.Q1686K. However, in our primary T cell activity assay, p.Q1686P, but not p.Q1686K, met criteria for abnormal activity. We also establish that many residues in TSC2 are partially tolerant to amino acid substitution, suggesting PM5 evidence should be used with caution for TSC2.

Our work has several limitations. First, VAMP-seq is a cDNA-based assay and therefore is not appropriate for examining potential splice-altering variants. SGE and cliPE, by contrast, are based on endogenous editing and thus can capture the effect of splicing variants. Relatively few ($n = 121$ total variants; $n = 26$ ClinVar VUS) variants examined here

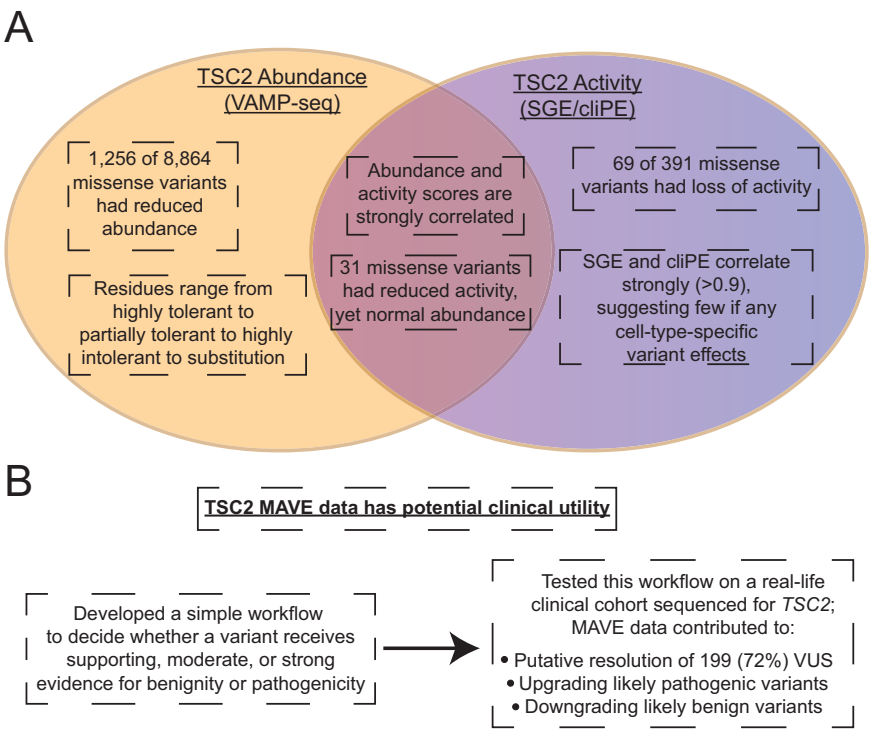

Fig. 8 | Summary of study findings. A Overview of significant findings from VAMP-seq abundance assay (in orange oval), TSC2 activity assays (SGE/cliPE in blue/purple gradient oval), and the relationships between abundance and activity (intersection of two ovals). **B** Summary of clinical utility of TSC2 MAVE data for variant classification.

have predicted splicing effects (SpliceAI Delta Score >0.2). We cannot rule out splicing effects for these particular variants as most ($n = 117$ variants) were only tested by VAMP-seq (Supplementary Table 1). Second, the TSC2 cDNA expressed in VAMP-seq may may not reflect endogenous levels of TSC2 expression. Third, we did not measure every possible mechanism of TSC2 variant pathogenicity, including the effect of variants on the TSC1-TSC2 interaction. Fourth, while both VAMP-seq and SGE are saturation approaches and therefore both prospective and retrospective, it is important to mention that cliPE is an inherently retrospective approach. In cliPE, we generate variant libraries based on clinically observed variants in databases such as ClinVar, LOVD, and gnomAD at one point in time. As more individuals are sequenced, we are likely to uncover novel variants in *TSC2*. Saturation approaches like VAMP-seq or SGE inherently provide data to help us understand these variants, whereas additional cliPE experiments would need to be performed to include such variants. We recommend cliPE as a good alternative to SGE when budget is a limiting factor; SGE should be considered if funding permits. Finally, low-passage HAP1 cells were used for cliPE, but we did not select for ploidy using flow cytometry or pharmacology[34,35]. We anticipate that, if any HAP1 cells spontaneously became diploid, this was unlikely to be a major confounding factor. If any individual cell became diploid after prime editing but before fixation, that cell would be homozygous with two copies of whichever TSC2 variant was initially present. If any cells became spontaneously diploid prior to prime editing, it is possible that they could be heterozygous with one variant allele and one reference allele or even compound heterozygous for two different variant alleles. It is likely that such cells would be a small minority of the cells in the assay and unlikely to significantly impact the final enrichment score for any particular variant. The clear separation between assay control variants (SYN and PTC) and ClinVar truth set variants (BLB and PLP) argue that this assay is not significantly confounded by ploidy (Figs. 2A and 6). We cannot rule out a small effect of ploidy on our assay results, particularly for putative partial loss-of-function variants or dominant negative variants. Our primary goal was developing a MAVE which could distinguish complete loss-of-function missense variants from variants retaining function. Future work will be necessary to develop assays that are calibrated to test for partial loss-of-function or dominant negative variants.

This study builds on the excellent work by the Nellist lab and others to functionally characterize individual missense variants in *TSC2*[13]. We have made our variant effect data available in the supplementary information (Supplementary Data 4 and 5). Our work is registered on the MAVE Registry and our data has been deposited in MAVEdb to share with the community[36,37]. Future directions of this work include forming a Clingen Variant Curation Expert Panel to generate a custom adaptation of the ACMG/AMP guidelines optimized for *TSC2*. It will be important to complete additional VAMP-seq, SGE, and cliPE studies to generate a complete variant effect map for the full *TSC2* gene.

Pathogenic variants in at least 16 mTOR pathway genes result in mTORopathies, a group of neurodevelopmental disorders commonly associated with epilepsy, in both children and adults[38]. We also view this study as a proof-of-concept towards comprehensive VUS resolution in the mTORopathies. The methods utilized herein are generalizable and could be used to study mTORopathy genes with missense VUS such as *DEPDC5*, *NPRL2*, or *NPRL3*, perhaps increasing access to mTOR inhibitors and other forms of precise clinical management.

Methods

TSC2 VAMP-seq

Barcoding attB_IRES-mCherry plasmid. The VAMP-seq vector was modified based on a previously described system (Supplementary Fig. 18)[39]. Briefly, an 18-nucleotide randomized sequence, flanked by BsmBI recognition sites and fragment-specific overhangs, was used as the barcode insert. This fragment was assembled into the plasmid backbone, containing the *attB*-IRES-mCherry cassette and a C-terminally GFP-tagged construct, via complementary overhangs with 1:7 vector:insert ratio. The resulting product was transformed by two electrocompetent NEB 10-beta E.coli cells (NEB C3020) reactions recovered in 2 mL SOC Media for one hour at 37 °C. Recovered cultures were plated to a 245 mm LB + AMP agar tray (Corning 07-200-600) and incubated at 30°C overnight. Plasmid DNA was then isolated by maxipreparation (Zymo Research D4203). Barcode diversity was estimated by colony counting, yielding 2.73e9 unique barcodes for subsequent library cloning.

Library cloning

Two site-saturation variant libraries were generated by Twist Biosciences based on the TSC2 open reading frame (NM_000548.5), C-terminally tagged with GFP. At each targeted site, we programmed a synonymous mutation, 19 missense mutations, a nonsense mutation, and a three base pair deletion. Library 1 is a site-saturation mutagenesis of amino acid residues 554-754 (187 sites passed QC) and library 2 is a site-saturation mutagenesis of amino acid residues 1512-1802 (286 sites passed QC). These two libraries were cloned to the above-mentioned barcoded plasmid using SapI golden gate cloning (NEB R0569S) followed by transformation by electroporation to achieve a barcode to variant coverage of 24× and 21×, respectively, for the two libraries. To associate barcodes with variants, we used PacBio SMRTbell sequencing. Libraries were prepared according to the manufacturer's protocol "Procedure & Checklist - Preparing SMRTbell® Libraries using PacBio® Barcoded Universal Primers for Multiplexing Amplicons." This resulted in 930,059 reads for Library 1 and 244,393 reads for Library 2. Barcodes were mapped to variants using Pacybara and only barcodes associated with a single unique variant at least two thirds of the time were used for VAMP-seq assays[40].

Tissue culture experiments and FACS sorting

Landing pad HEK 293T (HEK293T-LLP-iCasp9) cells were transfected using FuGene 6 with each barcoded variant library to achieve an estimated 20 cells per barcode coverage[41]. At 48 h post-transfection, cells with successful Bxb1-mediated integration were induced with 2 µg/mL doxycycline in media (DMEM + 10% FBS + 1% penicillin-streptomycin). After an additional 24 h, cells were treated with 10 nM of AP1903/Rimiducid (MedChemExpress) to select against unrecombined cells. At day 4 post-transfection, cells were sorted on a BD FACSAriaII using an 85 µm or 100 µm nozzle into four bins (Bin 1: 0–25%; Bin 2: 25–50%; Bin 3: 50–75%; Bin 4: 75–100%) based on GFP:mCherry fluorescence via FACS to achieve at least two million cells per bin[42]. Following sorting, the separate bins were grown out for several days to confluence in media (+ doxycycline) prior to harvesting genomic DNA from cell pellets (300 × *g* for 5 min).

Genomic DNA isolation and barcode sequencing

Genomic DNA was extracted from cell pellets of each bin using the Qiagen DNeasy Blood & Tissue Kit (Qiagen #695060) following the recommended protocol for purification of total DNA from animal blood or cells (spin-column protocol using a maximum of five million cells per column), with the addition of 2 µL RNase A (20 mg/mL) in the lysis step.

Two technical PCR replicates were performed following previously described protocols on each bin for each library to assess barcode correlation from amplification and sequencing[42,43].

Each indexed sample was sequenced for barcodes using custom read and indexing sequencing primers NP0494, NP0495; NP0497, and NP0550 using a NextSeq 1000/2000 P3 50 cycles kit (Illumina). All VAMP-seq oligonucleotide sequences are provided in Supplementary Data 6.

VAMP-seq data analysis and scoring

Variants were scored using previously published methods[21]. Briefly, fastq files were generated using bcl2fastq v2.20 and paired reads were merged using PEAR v0.9.11. Using CountESS 0.1.16 (https://countess-project.github.io/CountESS/), fastq reads were mapped to barcodes from the Pacybara output and collapsed to generate count tables where each row represents a variant and each column is a single bin in a replicate experiment. Variant frequencies within each bin ($F_{v,binx}$) were calculated by dividing the count for that variant by the sum of all counts in that bin. Bin frequency values were used to generate weighted abundance scores (W_v) for each variant by taking the frequency in bin 1 and multiplying by 0.25, bin 2 by 0.5, bin 3 by 0.75, and bin 4 by 1 and summing those values before dividing by the unweighted sum for that variant across all bins (1).

$$W_v = \frac{(F_{v,bin1} \times 0.25) + (F_{v,bin2} \times 0.5) + (F_{v,bin3} \times 0.75) + (F_{v,bin4} \times 1)}{(F_{v,bin1} + F_{v,bin2} + F_{v,bin3} + F_{v,bin4})} \quad (1)$$

Weighted average values range from 0.25 to 1 before normalization. Weighted average values were min-max normalized to develop an abundance score (S_v) such that WT (TSC2 reference allele) is equal to 1 and the median of the lowest 5% of missense values is equal to 0 to generate the reported abundance scores (2). We use the term abundance specifically to refer to the amount of protein present in each cell at steady-state.

$$Sv = \frac{W_v - \tilde{x}_{Wv,lowMissense}}{W_{WT} - \tilde{x}_{Wv,lowMissense}} \quad (2)$$

All VAMP-seq scores are reported in Supplementary Data 4 and 5. Variant to barcode maps and.ini configuration files for reproducing the CountESS pipeline are available at the following repository: https://github.com/FowlerLab/TSC2_analysis/tree/TSC2_manuscript. Reproducibility is demonstrated in replicate scatterplots (Supplementary Fig. 19).

Primary T cell saturation genome editing

The cloning-free SGE workflow described below, as previously described for *CARD11*, is shown in Supplementary Fig. 20[23].

SGE library design

Single-stranded oligonucleotide pool variant libraries (IDT oPools) were designed to include all possible single-nucleotide variants across each SGE region (Supplementary Data 7). Each oligonucleotide incorporated three synonymous guide-blocking edits within the protospacer and PAM site to prevent Cas9 re-cutting. Homology arms were added to both ends of the SGE region such that the entire length of each oligonucleotide was approximately 145 bases. Oligonucleotides also contained phosphorothioate bonds between the three terminal bases to inhibit degradation.

CD4$^+$ T cell isolation, activation, and culture conditions

Deidentified human peripheral blood mononuclear cells were acquired from healthy donors under informed consent from the Fred Hutch Specimen Processing and Research Cell Bank (protocol #3942). CD4$^+$ T cells were isolated (Fred Hutchinson Cancer Research Center) using the EasySep Human CD4$^+$ T cell enrichment kit (Stem Cell Technologies 19052). Cells were cultured at a density of 0.5e6 cells/mL in RPMI (ThermoFisher) supplemented with 20% FBS (Sigma), 1x Glutamax (ThermoFisher), 10 mM HEPES (ThermoFisher), 0.1% BME (ThermoFisher) and 50 ng/mL IL-2 (PeproTech). For activation, Dynabeads Human T-Expander CD3/28 (ThermoFisher) were added at 30 µL/1e6 cells. Beads were removed after 72 h, and cells were allowed to rest and proliferate for 16–20 h before transfection.

Transfection of CD4$^+$ T cells

CRISPR RNA (100 µM; IDT) was complexed with 100 µM trRNA (IDT) at a ratio of 1:1 and incubated at 95 °C for 5 min, then allowed to cool at room temperature for 30–60 min. Recombinant Cas9 (UC Berkeley) was added at a guide:Cas9 molar ratio of 4:1 and the mixture was allowed to rest at room temperature for 15 min. Single-stranded oligonucleotide variant libraries were added at a final concentration of 40 pmol/1e6 cells. CD4+ cells were resuspended in Maxcyte buffer (Maxcyte) and added to the Cas9/guide/library mix. This sample was then transferred to a Maxcyte assembly and transfected with the Expanded T Cell-1 protocol on a Maxcyte ExPERT GTx electroporator.

Cell staining and sorting

Following transfection, cells were cultured for 6 days with media replacement every 48 h. Approximately 1e6 cells were isolated for downstream genomic DNA and the remaining cells were fixed, permeabilized, and stained for phosphorylated S6 (Cell Signaling Technology 5316S). Stained cells were analyzed on a BD FACSAria II flow cytometer and cells were sorted on the highest and lowest 25% of phospho-S6 intensity. An example histogram from one sort is shown in Supplementary Fig. 20B.

Genomic DNA isolation

Genomic DNA was isolated from presorted cells using the Quick-DNA miniprep kit (Zymo Research). For fixed cells, cell pellets containing approximately 1-2e6 cells were suspended in 250 µL of PBS containing 200 µg of RNAse A (Sigma) and 200 µg Proteinase K (Zymo Research). Cells were incubated at 37 °C for 30 min. Lysis buffer (250 µL at 2×) containing 60 mM Tris pH 8, 20 mM EDTA, and 2% SDS was added and cells were incubated overnight at 65 °C with shaking at 800 rpm. Ethanol (250 µL) was then added to the sample and genomic DNA was isolated with the Quick-DNA miniprep kit.

Illumina sequencing

Each SGE region was first amplified with intron-specific primers amplifying the entire exonic region with NEBNext Ultra II Q5 high fidelity DNA polymerase (New England Biolabs) (Supplementary Data 8). This sample was then purified with Agencourt AMPure XP reagent (Beckman Coulter) at a 0.9× beads to sample ratio. These samples were then amplified with locus-specific primers containing Illumina adapter sequences. These samples were purified with 0.9× AMPure beads and reamplified with primers containing Illumina p5 and p7 sequences and a unique sample index. These samples were purified one final time with 0.9x AMPure beads. The amplicon library was verified for purity by PAGE gel, quantified by Qubit 3 (ThermoFisher), pooled, and paired-end sequenced on an Illumina NextSeq 2000 with the XLEAP P2 300 cycle kit (Illumina).

Data analysis and scoring

After Illumina sequencing, individual replicates ($n = 4$ replicates: 2 donors, 2 replicates each donor) were de-multiplexed and Illumina reads were merged with the PEAR software package. We then used custom Python scripts to isolate and count variants in the paired-end reads for the pS6-Hi and pS6-Lo populations. We then used the CountESS software package to generate functional scores. Briefly, variant counts within each sample were normalized by dividing the count of each individual variant by the total variant counts observed in that sample. Replicate scores were then calculated as the ratio of normalized variant counts in the pS6-Hi population to that of the pS6-Lo population. To enable comparisons across regions, scores were scaled within each region using internal reference points. Specifically, the mean of the three lowest scoring variants and the mean of the three highest scoring variants in each region were used to define the minimum and maximum, respectively, and scores were linearly rescaled between these bounds. Finally, within each region, variant scores were

normalized to the average score of the synonymous variants from the same region. All SGE scores are reported in Supplementary Data 4 and 5 and Supplementary Table 1. Editing rates are shown in Supplementary Fig. 21 and reproducibility demonstrated in replicate scatterplots in Supplementary Fig. 22.

Curated loci prime editing

cliPE is a modification of a published method for saturation prime editing[44]. For a detailed cliPE protocol, please see Biar et al. or the supplementary methods[24]. Briefly, enhanced prime editing guide RNA (epegRNA) libraries were cloned into a mammalian expression construct with a U6 promoter (Supplementary Fig. 23). epegRNA libraries were co-transfected into HAP1 cells with plasmids expressing the PEmax prime editor as well as nicking gRNAs to enhance editing efficiency. After selection for PEmax-expressing cells via FACS sorting for GFP+ cells, cells were serum starved overnight prior to trypsinization, fixation, and immunolabeling for pS6. High pS6 (upper quartile) cells were sorted and collected. In addition, unsorted cells were collected. Amplicon sequencing was used to quantify allele frequency in sorted and unsorted cells and an enrichment score for TSC2 activity was computed from the allele frequency within high pS6 cell pools divided by the allele frequency in unsorted cell pools. All cliPE scores are reported in Supplementary Data 4 and 5. Reproducibility is demonstrated in replicate scatterplots in Supplementary Fig. 24.

Correlation analysis

To investigate the correlation between our MAVE-derived variant effect scores and either measures of evolutionary conservation or variant effect predictors, we used the Ensemble VEP package to annotate variants scored in our assays with scores available in the dbNSFP database[45–47]. We selected GERP, phastCons, and phyloP as three different algorithms which measure evolutionary conservation using multiple sequence alignments[48–50]. GERP++ and phyloP are more similar as they are column-based measures which generate a score based on a single position within the alignment. phastCons differs in its approach as it incorporates flanking columns as additional context. We selected the following variant effect predictors (VEPs): (1) AlphaMissense, (2) BayesDel (with or without allele frequency), (3) ClinPred, (4) MutPred2, (5) PrimateAI, (6) REVEL, (7) VARITY, (8) gMVP, and (9) EVE[27,51–57]. The VEPs are a mix of the three different VEP categories as defined by Livesey and Marsh, with AlphaMissense and PrimateAI being "Population-tuned", EVE being "Population-free", and the remaining being "Clinical-trained"[25]. "Clinical-trained" VEPs use a training set of variants with known clinical labels or incorporate a feature which has been trained on such a variant set. "Population-free" VEPs do not use any clinical labels or population data and rather rely on other features such as multiple sequence alignment. "Population-tuned" VEPs incorporate human population genetic data in some form during model development. All pairwise correlations are provided in Supplemental Data 9, 10.

MAVE thresholds and OddsPath calibration

Thresholds for normal and abnormal abundance or activity for each MAVE were primarily determined by receiver operating characteristic (ROC) analysis using the pROC package[58]. We used the Youden statistic to determine the threshold which best separated known ClinVar BLB and PLP missense variants for each assay. For VAMP-seq, variants with abundance <0.25 were determined to have abnormal (low) abundance. Variants with an abundance score between 0.25 and 0.75 met the criteria for indeterminate abundance. Variants with abundance scores >0.75 were determined to have normal abundance, coinciding with the lower 95% confidence interval for synonymous variants in the VAMP-seq assay. For SGE and cliPE, we developed single thresholds to classify variants as either having normal or abnormal activity. For SGE, variants with TSC2 activity scores <2 were classified as having normal activity, while variants with scores >2 were classified as having abnormal activity. For cliPE, variants with TSC2 activity scores <0.25 were classified as having normal activity, while variants with scores >0.25 were classified as having abnormal activity. For all assays, OddsPath calculations were performed using the current ClinGen-approved calibration framework (Table 2)[30]. The OddsPath calculation is based on the proportion of pathogenic variants in the truth set as a prior probability (P_1) and the proportion of pathogenic variants in the functionally abnormal MAVE dataset based on the above thresholds as a posterior probability (P_2) (3):

$$OddsPath = \frac{[P_2 \times (1 - P_1)]}{[(1 - P_2) \times P_1]} \quad (3)$$

Variant classification on Ambry cohort

This study was reviewed and approved by the University of Washington Institutional Review Board (IRB#3598). Preliminary Ambry classifications for *TSC2* missense variants that have been observed in individuals tested at Ambry genetics ($n = 340$) were performed utilizing the Ambry Classifi framework based on ACMG/AMP guidelines and implementing a points-based approach[28,59]. Diagnostic criteria for application of phenotype-based evidence was based on international consensus criteria[60]. Population-based evidence thresholds were established within Ambry's Classifi program using gene-specific Whiffin-Ware calculations[61]. For the final classifications, in silico prediction-based points were assigned based on AlphaMissense thresholds that were calibrated for *TSC2* and functional weight was incorporated using the calibrated points-based approach described in Table 2 (range of −2 to 4)[28,30]. Detailed phenotypic information on a per variant basis is provided in Supplementary Data 11.

Variant classification on all other missense variants assayed

A simplified version of the points-based system used for the Ambry cohort was used for variants that had not been previously observed in the Ambry cohort. Where available, a calibrated in silico predictor optimized for *TSC2* was generated from AlphaMissense scores[62]. Based on the strength of evidence calculated for the functional datasets (Table 2), variants were assigned a range of points between −2 and +4[30].

Reporting summary

Further information on research design is available in the Nature Portfolio Reporting Summary linked to this article.

Data availability

VAMP-seq data is available via: IGVF Portal [https://data.igvf.org/analysis-sets/IGVFDS5595BTYJ/] (Analysis set: IGVFDS5595BTYJ). Github [https://doi.org/10.5281/zenodo.20837253] (Zenodo archived release of Github repo: https://github.com/FowlerLab/TSC2_analysis). SGE data is available via: IGVF Portal [https://data.igvf.org/analysis-sets/IGVFDS1782FCXW/] (Analysis set: IGVFDS1782FCXW). cliPE data is available via: MAVEdb [https://www.mavedb.org/score-sets/urn:mavedb:00001201-a-1] (urn:mavedb:00001201-a). NCBI Sequence Read Archive [https://www.ncbi.nlm.nih.gov/bioproject/PRJNA1422769] (PRJNA1422769). Scoresets are also provided in Supplementary Data 4 and 5. Source data are provided with this paper.

Code availability

Code to perform quality control (QC) filtering on *TSC2* VAMP-seq variant abundance scores by applying a read-count frequency threshold at the variant level across biological replicates is provided: Github [https://doi.org/10.5281/zenodo.20837253] (Zenodo archived release of Github repo: https://github.com/FowlerLab/TSC2_analysis).

References

1. van Slegtenhorst, M. et al. Identification of the tuberous sclerosis gene TSC1 on chromosome 9q34. *Science* **277**, 805–808 (1997).
2. European Chromosome 16 Tuberous Sclerosis Consortium. Identification and characterization of the tuberous sclerosis gene on chromosome 16. *Cell* **75**, 1305–1315 (1993).
3. Green, R. C. et al. ACMG recommendations for reporting of incidental findings in clinical exome and genome sequencing. *Genet. Med.* **15**, 565–574 (2013).
4. Huang, J. & Manning, B. D. The TSC1-TSC2 complex: a molecular switchboard controlling cell growth. *Biochem. J.* **412**, 179–190 (2008).
5. Inoki, K., Li, Y., Xu, T. & Guan, K.-L. Rheb GTPase is a direct target of TSC2 GAP activity and regulates mTOR signaling. *Genes Dev.* **17**, 1829–1834 (2003).
6. Hodges, A. K. et al. Pathological mutations in TSC1 and TSC2 disrupt the interaction between hamartin and tuberin. *Hum. Mol. Genet.* **10**, 2899–2905 (2001).
7. Ramlaul, K. et al. Architecture of the tuberous sclerosis protein complex. *J. Mol. Biol.* **433**, 166743 (2021).
8. Yang, H. et al. Structural insights into TSC complex assembly and GAP activity on Rheb. *Nat. Commun.* **12**, 339 (2021).
9. Hansmann, P. et al. Structure of the TSC2 GAP domain: Mechanistic insight into catalysis and pathogenic mutations. *Structure* **28**, 933–942.e4 (2020).
10. Schwartz, R. A., Fernández, G., Kotulska, K. & Jóźwiak, S. Tuberous sclerosis complex: advances in diagnosis, genetics, and management. *J. Am. Acad. Dermatol.* **57**, 189–202 (2007).
11. Staley, B. A., Vail, E. A. & Thiele, E. A. Tuberous sclerosis complex: diagnostic challenges, presenting symptoms, and commonly missed signs. *Pediatrics* **127**, e117–e125 (2011).
12. He, W. et al. Sirolimus improves seizure control in pediatric patients with tuberous sclerosis: A prospective cohort study. *Seizure* **79**, 20–26 (2020).
13. Hoogeveen-Westerveld, M. et al. Functional assessment of TSC2 variants identified in individuals with tuberous sclerosis complex. *Hum. Mutat.* **34**, 167–175 (2013).
14. Dufner Almeida, L. G. et al. Comparison of the functional and structural characteristics of rare TSC2 variants with clinical and genetic findings. *Hum. Mutat.* **41**, 759–773 (2020).
15. Hoogeveen-Westerveld, M. et al. Functional assessment of variants in the TSC1 and TSC2 genes identified in individuals with Tuberous Sclerosis Complex. *Hum. Mutat.* **32**, 424–435 (2011).
16. Dufner-Almeida, L. G. et al. Molecular and functional assessment of TSC1 and TSC2 in individuals with tuberous sclerosis complex. *Genes* **15**, 1432 (2024).
17. Coevoets, R. et al. A reliable cell-based assay for testing unclassified TSC2 gene variants. *Eur. J. Hum. Genet.* **17**, 301–310 (2009).
18. Rosengren, T. et al. Mutational analysis of TSC1 and TSC2 in Danish patients with tuberous sclerosis complex. *Sci. Rep.* **10**, 9909 (2020).
19. Nellist, M. et al. Functional characterisation of the TSC1-TSC2 complex to assess multiple TSC2 variants identified in single families affected by tuberous sclerosis complex. *BMC Med. Genet.* **9**, 10 (2008).
20. McEwen, A. E., Tejura, M., Fayer, S., Starita, L. M. & Fowler, D. M. Multiplexed assays of variant effect for clinical variant interpretation. *Nat. Rev. Genet.* https://doi.org/10.1038/s41576-025-00870-x (2025).
21. Matreyek, K. A. et al. Multiplex assessment of protein variant abundance by massively parallel sequencing. *Nat. Genet.* **50**, 874–882 (2018).
22. Calhoun, J. D. et al. mTORC1 functional assay reveals SZT2 loss-of-function variants and a founder in-frame deletion. *Brain* **145**, 1939–1948 (2022).
23. Meitlis, I. et al. Multiplexed Functional Assessment of Genetic Variants in CARD11. *Am. J. Hum. Genet.* **107**, 1029–1043 (2020).
24. Biar, C. G., Bodkin, N., Carvill, G. L. & Calhoun, J. D. Protocol to perform multiplexed assays of variant effect using curated loci prime editing. *STAR Protoc.* **6**, 103851 (2025).
25. Livesey, B. J. & Marsh, J. A. Variant effect predictor correlation with functional assays is reflective of clinical classification performance. *Genome Biol.* **26**, 104 (2025).
26. Schulze, T. K. & Lindorff-Larsen, K. Effects of residue substitutions on the cellular abundance of proteins. *eLife* https://doi.org/10.7554/elife.103721.2 (2026).
27. Cheng, J. et al. Accurate proteome-wide missense variant effect prediction with AlphaMissense. *Science* **381**, eadg7492 (2023).
28. Richards, S. et al. Standards and guidelines for the interpretation of sequence variants: a joint consensus recommendation of the American College of Medical Genetics and Genomics and the Association for Molecular Pathology. *Genet. Med.* **17**, 405–424 (2015).
29. Harrison, S. M. et al. Clinical laboratories collaborate to resolve differences in variant interpretations submitted to ClinVar. *Genet. Med.* **19**, 1096–1104 (2017).
30. Brnich, S. E. et al. Recommendations for application of the functional evidence PS3/BS3 criterion using the ACMG/AMP sequence variant interpretation framework. *Genome Med.* **12**, 3 (2019).
31. Previtali, R. et al. Paradigm shift in the treatment of tuberous sclerosis: Effectiveness of everolimus. *Pharmacol. Res.* **195**, 106884 (2023).
32. Luo, C. et al. Low-dose everolimus maintenance therapy for renal angiomyolipoma associated with tuberous sclerosis complex. *Front. Med.* **8**, 744050 (2021).
33. Luo, C. et al. Renal phenotypes correlate with genotypes in unrelated individuals with tuberous sclerosis complex in China. *Orphanet J. Rare Dis.* **17**, 288 (2022).
34. Olbrich, T. et al. A chemical screen identifies compounds capable of selecting for haploidy in mammalian cells. *Cell Rep.* **28**, 597–604.e4 (2019).
35. Beigl, T. B., Kjosås, I., Seljeseth, E., Glomnes, N. & Aksnes, H. Efficient and crucial quality control of HAP1 cell ploidy status. *Biol. Open* **9**, bio057174 (2020).
36. Kuang, D. et al. MaveRegistry: a collaboration platform for multiplexed assays of variant effect. *Bioinformatics* **37**, 3382–3383 (2021).
37. Esposito, D. et al. MaveDB: an open-source platform to distribute and interpret data from multiplexed assays of variant effect. *Genome Biol.* **20**, 223 (2019).
38. Moloney, P. B., Cavalleri, G. L. & Delanty, N. Epilepsy in the mTORopathies: opportunities for precision medicine. *Brain Commun.* **3**, fcab222 (2021).
39. Amorosi, C. J. et al. Massively parallel characterization of CYP2C9 variant enzyme activity and abundance. *Am. J. Hum. Genet.* **108**, 1735–1751 (2021).
40. Weile, J. et al. Pacybara: accurate long-read sequencing for barcoded mutagenized allelic libraries. *Bioinformatics* **40**, btae182 (2024).
41. Matreyek, K. A., Stephany, J. J., Chiasson, M. A., Hasle, N. & Fowler, D. M. An improved platform for functional assessment of large protein libraries in mammalian cells. *Nucleic Acids Res.* **48**, e1 (2020).
42. Wang, R. & Wheelock, M. VAMPseq Protocol. Preprint at https://www.protocols.io/view/vampseq-protocol-4r3l2q77xl1y/v1 (2024).
43. Popp, N. A. et al. Multiplex and multimodal mapping of variant effects in secreted proteins via MultiSTEP. *Nat. Struct. Mol. Biol.* **32**, 2099–2111 (2025).
44. Erwood, S. et al. Saturation variant interpretation using CRISPR prime editing. *Nat. Biotechnol.* **40**, 885–895 (2022).

45. McLaren, W. et al. The Ensembl Variant Effect Predictor. *Genome Biol.* **17**, 122 (2016).
46. Liu, X., Jian, X. & Boerwinkle, E. dbNSFP: a lightweight database of human nonsynonymous SNPs and their functional predictions. *Hum. Mutat.* **32**, 894–899 (2011).
47. Liu, X., Li, C., Mou, C., Dong, Y. & Tu, Y. dbNSFP v4: a comprehensive database of transcript-specific functional predictions and annotations for human nonsynonymous and splice-site SNVs. *Genome Med.* **12**, 103 (2020).
48. Davydov, E. V. et al. Identifying a high fraction of the human genome to be under selective constraint using GERP++. *PLoS Comput. Biol.* **6**, e1001025 (2010).
49. Siepel, A. et al. Evolutionarily conserved elements in vertebrate, insect, worm, and yeast genomes. *Genome Res.* **15**, 1034–1050 (2005).
50. Pollard, K. S., Hubisz, M. J., Rosenbloom, K. R. & Siepel, A. Detection of nonneutral substitution rates on mammalian phylogenies. *Genome Res.* **20**, 110–121 (2010).
51. Tian, Y. et al. REVEL and BayesDel outperform other in silico meta-predictors for clinical variant classification. *Sci. Rep.* **9**, 12752 (2019).
52. Alirezaie, N., Kernohan, K. D., Hartley, T., Majewski, J. & Hocking, T. D. ClinPred: Prediction tool to identify disease-relevant nonsynonymous single-nucleotide variants. *Am. J. Hum. Genet.* **103**, 474–483 (2018).
53. Pejaver, V. et al. Inferring the molecular and phenotypic impact of amino acid variants with MutPred2. *Nat. Commun.* **11**, 5918 (2020).
54. Sundaram, L. et al. Predicting the clinical impact of human mutation with deep neural networks. *Nat. Genet.* **50**, 1161–1170 (2018).
55. Wu, Y., Li, R., Sun, S., Weile, J. & Roth, F. P. Improved pathogenicity prediction for rare human missense variants. *Am. J. Hum. Genet.* **108**, 1891–1906 (2021).
56. Zhang, H., Xu, M. S., Fan, X., Chung, W. K. & Shen, Y. Predicting functional effect of missense variants using graph attention neural networks. *Nat. Mach. Intell.* **4**, 1017–1028 (2022).
57. Frazer, J. et al. Disease variant prediction with deep generative models of evolutionary data. *Nature* **599**, 91–95 (2021).
58. Robin, X. et al. pROC: an open-source package for R and S+ to analyze and compare ROC curves. *BMC Bioinforma.* **12**, 77 (2011).
59. Tavtigian, S. V., Harrison, S. M., Boucher, K. M. & Biesecker, L. G. Fitting a naturally scaled point system to the ACMG/AMP variant classification guidelines. *Hum. Mutat.* **41**, 1734–1737 (2020).
60. Northrup, H. et al. Updated International tuberous sclerosis complex diagnostic criteria and surveillance and management recommendations. *Pediatr. Neurol.* **123**, 50–66 (2021).
61. Whiffin, N. et al. Using high-resolution variant frequencies to empower clinical genome interpretation. *Genet. Med.* **19**, 1151–1158 (2017).
62. Tejura, M. et al. Calibration of variant effect predictors on genome-wide data masks heterogeneous performance across genes. *Am. J. Hum. Genet.* **111**, 2031–2043 (2024).

Acknowledgements

This work was supported by the Northwestern University – Flow Cytometry Core Facility supported by Cancer Center Support Grant (NCI CA060553). Flow Cytometry Cell Sorting was performed on a BD FACSAria SORP system and BD FACSymphony S6 SORP system, purchased through the support of NIH 1S10OD011996-01 and 1S10OD026814-01. We thank David Liu and the Liu lab for sharing their prime editing reagents. The authors would like to acknowledge Addgene for its invaluable service which facilitated this study. We further thank the Plasmidsaurus sequencing team for making quality control and pilot experiments more feasible and accessible.

Author contributions

Conceptualization: G.L.C., J.D.C., R.J., D.F., L.M.S. Investigation: C.G.B., J.D.C., Z.R.W., N.D.C., M.K.W., S.P., A.V.M., A.J.V., S.D. Visualization: D.L.H., J.D.C. Formal analysis: D.L.H., N.D.C., J.D.C. Data curation: A.F.R., N.M., P.G., A.M., J.D.W., M.E.R., T.C., R.S., D.Z., P.R., M.T. Project administration: G.L.C., R.J., D.F., L.M.S., J.D.C. Writing—original draft: J.D.C. Writing—editing: J.D.C., P.G., A.M., J.D.W., M.E.R., T.C., N.D.C., R.J., D.L.H., L.M.S., C.G.B.

Funding

This work was sponsored by an American Epilepsy Society Junior Investigator Award (J.D.C.) and a TSC Alliance Research Grant (J.D.C.). This work was supported by the NIH NHGRI IGVF Program (HG011969). A.V.M. was supported in part by National Human Genome Research Institute Interdisciplinary Training in Genome Sciences Grant T32HG000035.

Competing interests

M.E.R, J.W. and T.C. are employees of Ambry Genetics. The remaining authors declare no competing interests.

Additional information

Supplementary information The online version contains supplementary material available at https://doi.org/10.1038/s41467-026-75442-6.

Correspondence and requests for materials should be addressed to Richard G. James, Douglas M. Fowler or Jeffrey D. Calhoun.

Peer review information *Nature Communications* thanks Willow Coyote-Maestas and the other, anonymous, reviewer(s) for their contribution to the peer review of this work. A peer review file is available.